Coupled Helicopter Rotor/Body Aeromechanical Stability Comparison of Theoretical and Experimental Results

P. P. Friedmann* and C. Venkatesan†
University of California, Los Angeles, California

This paper presents the results of an analytical study aimed at predicting the aeromechanical stability of a helicopter in ground resonance, with the inclusion of aerodynamic forces. The theoretical results are found to be in good agreement with the experimental results, available in the literature, indicating that the coupled rotor/fuselage system can be represented by a reasonably simple mathematical model.

Nomenclature

a = lift curve slope
b = blade semichord
$C(k)$ = Theodorsen's lift deficiency
C_{d0} = profile drag coefficient of the blade
e = hinge offset
f = rotating natural frequency
g_{SF}, g_{SL} = structural damping in flap and lag degrees of freedom, respectively
h_2 = height of rotor hub above the gimbal
$I_{xx}, I_{xy}, I_{yy}, I_{yx}$ = rotary inertia of the model about the gimbal axes
K_β, K_ζ = stiffness of the root springs of the blade in flap and lag, respectively
ℓ = length of blade, $= R - e$
m = mass/unit length of the blade
N = number of blades
n = harmonic index
R = rotor radius
s = complex eigenvalue
t = time
β_{nc}, β_{ns} = n cosine, n sine flap coordinates
β_p = blade precone, in equations
β_p = progressing flap mode (high frequency) in figures
β_R = regressing flap mode (low frequency)
β_0 = rotor blade equilibrium angle in flap
β_{1c}, β_{1s} = cyclic flap coordinates
$\Delta\beta_k$ = time-dependent perturbations of the kth blade in flap
ϵ = order of magnitude used for ordering various quantities
ζ_p = progressing lag mode (high frequency)
ζ_R = regressing lag mode (low frequency)
ζ_{1c}, ζ_{1s} = cyclic lag coordinates
ζ_0 = rotor blade equilibrium angle in lag
$\Delta\zeta_k$ = time-dependent perturbations of the kth blade in lag
ζ_{nc}, ζ_{ns} = n cosine, n sine lag coordinates
θ = body pitch
θ_c = collective pitch setting of the blade
$\theta_{\text{eff}}, \theta_0$ = effective angle of attack
θ_{ZL} = zero lift angle of attack
λ = inflow ratio
ν = $\rho_A abR/m$
ρ_A = density of air
σ = modal damping (real part of s)
$\bar{\sigma}$ = solidity ratio
ϕ = body roll
ψ = nondimensional time (Ωt)
ω = modal frequency (imaginary part of s)
Ω = rotor rpm
$\bar{\omega}_F$ = nondimensional, nonrotating flap frequency, $[K_\beta/(m\Omega^2 R^3)]^{1/2}$
$\bar{\omega}_L$ = nondimensional, nonrotating lag frequency, $[K_\zeta/(m\Omega^2 R^3)]^{1/2}$

Superscripts

$(\bar{\ })$ = nondimensionalized quantity, with respect to R when involving length, and with respect to Ω when involving frequency
$(\dot{\ })$ = $\mathrm{d}/\mathrm{d}\psi$

Introduction

THE aeromechanical instability of a helicopter, on the ground and in flight, is caused by coupling between the rotor and the body degrees of freedom. This instability is commonly denoted air resonance when the helicopter is in flight and ground resonance when the helicopter is on the ground. The physical phenomenon associated with this instability is quite complex. The rotor lead-lag regressing mode usually couples with the body pitch or roll to cause the instability. The nature of the coupling which is both aerodynamic and inertial is introduced in the rotor by body or support motion. Development of a mathematically consistent model capable of representing the coupled rotor/fuselage dynamic system is of a fundamental importance for the study of this class of problems. The mathematical model should be consistent because the geometrically nonlinear terms associated with moderate blade deflections are known to have a significant role in rotary wing aeroelasticity.[1] Thus, various terms having the same order of magnitude must be retained throughout the derivation of the equations of motion. A consistent mathematical model has been developed[2,3] by the authors to study the aeroelastic, structural dynamic, and aeromechanical effects in multirotor systems.

Bousman[4] has obtained excellent experimental data for aeromechanical stability of a hingeless rotor on a special gimbaled support simulating body pitch and roll degrees of freedom. The availability of this high-quality experimental data provides an opportunity for comparing the results obtained from the analytical model with this experimental data. Bousman attributed some of the discrepancies found between the theoretical results presented in his paper and experimental

Received Nov. 7, 1983; revision received July 6, 1984.

*Professor, Mechanical, Aerospace and Nuclear Engineering Department. Associate Fellow AIAA.
†Assistant Research Engineer.

results to dynamic inflow. This conclusion was also examined by Johnson[5] in a recent study, where unsteady aerodynamic effects on the rotor were represented by a perturbation inflow model.[6] Johnson showed that, based on his model,[7] theoretical results with dynamic inflow provided results which showed better agreement with the experimental results than the results based on a quasisteady aerodynamic model without dynamic inflow. He concluded from his study that unsteady aerodynamic effects are represented quite well by a dynamic inflow model.

Using the mathematical model developed by the authors,[2,3] it is shown that the theoretical results, based on the quasisteady aerodynamic model, are, for most cases, in better agreement with the experimental results than the agreement noted by Bousman.[4] The agreement with the experimental data is also comparable to that obtained by Johnson,[5] except that the quasisteady model is incapable of predicting the "dynamic inflow mode" found by Johnson,[5] which is a result of the augmented state due to inflow dynamics.

This paper has a number of objectives:

1) It describes a set of relatively simple and carefully derived coupled rotor/fuselage equations[3] which yield good agreement with experimental data.

2) It shows that for the *zero* pitch settings of the blade, the agreement between theory and experiment is comparable to Ref. 5, except that the "dynamic inflow mode"[5] is not predicted. This limitation is due to the quasisteady aerodynamics used in our model.

3) It shows that for *nonzero* collective pitch settings of the blade, the theoretical results exhibit good agreement with the experimental data. The analytical model used in Ref. 4 showed poor correlation with experimental data, for lag regressing mode damping at nonzero pitch setting, and the comparisons in Ref. 5 were restricted to zero pitch setting. Hence, it is evident that this study provides correlation with experiments in a regime where no such correlation has been documented in the literature.

The good agreement between the analytical and experimental results indicates that the relatively simple analytical model is accurate for this case. Furthermore it also implies that only part of the discrepancy between theory and experiment, found by Bousman, may be attributed to dynamic inflow.

A Brief Summary of the Experiment

A clear description of the experimental setup, used for simulating the fundamental aspects of the aeromechanical stability of a hingeless rotor helicopter, is presented in Ref. 4. The rotor consisted of three blades and five different configurations were tested. The different configurations represent different blade parameters characterized by the nonrotating natural frequencies of the blade in flap and lag, pitch-lag coupling, and flap-lag coupling. The rotor was designed such that most of the blade flexibility is concentrated at the root by building in root flexures. The rotor assembly was supported on a gimbal which has pitch and roll degrees of freedom. In this paper the analytical results obtained were compared with the experimental results, presented by Bousman for rotor Configurations 1 and 4, where the designation of these configurations is consistent with those in Bousman's paper.[4] A brief description of these configurations is presented for the sake of completeness; additional information can be found in Refs. 4, 5, and 8. Configuration 1 had different stiffnesses in flap and lag, respectively; the corresponding nonrotating flap frequency was 3.13 Hz and that for lead-lag was 6.70 Hz. Configuration 4 was a matched stiffness case where the nonrotating flap frequency was 6.63 Hz and that for lead-lag was 6.73 Hz. The pitch-flap and pitch-lag couplings for these two configurations were zero. For cases where the pitch angle was nonzero, the experimental rotor was designed such that pitch changes were introduced outboard of the flexures and, therefore, the structural flap-lag coupling for these cases was zero. The blade was also designed to be very stiff in torsion. The data used in the calculations presented herein are presented in Table 1.

Description of the Analytical Model

The analytical model used to study this aeromechanical stability problem is based on the equations developed for a multirotor system presented in Refs. 2 and 3. These equations represent the dynamics of the coupled rotor/vehicle system consisting of two rotors interconnected by a flexible structure. The various degrees of freedom considered in deriving the equations are flap, lag, and torsion for each blade; rigid-body translation and rotation of the complete vehicle; and also the degrees of freedom representing the normal modes of vibration of the supporting structure. From this multirotor analytical model, only those degrees of freedom and the corresponding equations of motion that are relevant for the present study have been retained. The most important assumptions used are:

1) The rotor consists of three or more blades.
2) The rotor is lightly loaded.
3) The rotor is in uniform inflow.
4) The rotor blade is modeled as a rigid blade with orthogonal springs located at the root of the blade (Fig. 1), where K_β and K_ζ represent the stiffness of the blade in flap and lag motions.
5) The aerodynamic model used in the analysis is a quasisteady version of Greenberg's[9] theory with $C(k) = 1$, with the inclusion of apparent mass terms.
6) The inflow ratio λ, used in the calculation of the aerodynamic loads, was evaluated from[6]

$$\lambda = (\bar{\sigma}a/16)\left[\sqrt{1 + (24\theta_{\text{eff}}/\bar{\sigma}a)} - 1\right] \tag{1}$$

Table 1 Rotor, blade, and body properties

Rotor geometry		
No. of blades	3	
Radius, cm	81.1	
Chord, cm	4.19	
Hinge offset, cm	8.51	
Blade airfoil	NACA 23012	
Profile drag coefficient	0.0079	
Lock No.	7.73	
Solidity ratio	0.0494	
Lift curve slope	2π	
Height of rotor hub above gimbal, cm	24.1	
Blade mass properties		
Blade mass (to flap flexure), g	209	
Blade mass centroid (Ref. flexure centerline), cm	18.6	
Blade flap inertia (Ref. flexure centerline), g·m^2	17.3	
Body frequency and damping		
Pitch frequency, Hz	2	
Roll frequency, Hz	4	
Damping in roll (% critical)	0.929	
Damping in pitch (% critical)	3.20	
Blade frequency and damping	Configuration 1	Configuration 4
Nonrotating flap frequency, Hz	3.13	6.63
Nonrotating lead-lag frequency, Hz	6.70	6.73
Damping in lead-lag (% critical)	0.52	0.53
Body mass properties		
Rotary inertia in pitch, g·m^2	633	
Rotary inertia in roll, g·m^2	183	

As indicated in Ref. 4, a cambered airfoil was used in the model rotor tested; thus

$$\theta_{\text{eff}} = \theta_c - \theta_{ZL} \tag{2}$$

The zero lift angle of attack, for the airfoil employed[4] (NACA 23012), was $\theta_{ZL} = -1.5$ deg.

As mentioned earlier, the equations of motion are nonlinear, because geometrical nonlinearities due to moderate deflection of the blade are included. Retention of the nonlinear terms is based upon an ordering scheme.[1,2] The blade degrees of freedom, representing blade slopes, are assigned an order of magnitude represented by a symbolic quantity ϵ, and are assumed to be of order $\mathcal{O}(\epsilon)$, where $0.1 < \epsilon < 0.15$. The fuselage degrees of freedom are assumed to be of a slightly smaller magnitude $\mathcal{O}(\epsilon^{3/2})$. As indicated in Ref. 1, this assumption is quite important for obtaining equations which are manageable from an algebraic point of view. The ordering scheme consists of neglecting terms of order $\mathcal{O}(\epsilon^2)$ when compared to order one, thus $1 + \mathcal{O}(\epsilon^2) \simeq 1$.

The degrees of freedom considered in this aeromechanical stability analysis are, respectively, the fundamental flap and lag modes for each blade, and the pitch and roll degrees of freedom of the body. In this class of problems, it has been established that the collective flap and lag modes do not couple with the body motion and, thus, these modes are not considered. Therefore, the total number of degrees of freedom governing the aeromechanical problem are six. These consist of: cyclic flap (β_{1c}, β_{1s}), cyclic lead-lag (ζ_{1c}, ζ_{1s}), body pitch (θ), and body roll (ϕ).

Method of Solution

The method of solution for the coupled rotor/fuselage problem follows essentially the procedure explained in Refs. 1 and 3. A brief outline of the procedure is given below.

The equations of motion for the coupled rotor/fuselage problem are usually nonlinear differential equations with periodic coefficients. The solution procedure used for obtaining the stability information is as follows.

1) The static equilibrium position, in hover, represented by β_0 and ζ_0, is obtained by imposing the requirement that all time derivatives in blade and fuselage degrees of freedom vanish. This yields a set of nonlinear algebraic equations which are solved using the Newton-Raphson technique.

2) The blade degrees of freedom are expressed as time-varying perturbations about the static equilibrium position, β_0 and ζ_0 for flap and lag, respectively,

$$\beta_k(\psi) = \beta_0 + \Delta\beta_k(\psi)$$

$$\zeta_k(\psi) = \zeta_0 + \Delta\zeta_k(\psi)$$

Substituting these into the nonlinear ordinary differential equations of motion and neglecting terms which contain the product of the perturbation terms, yields the linearized equations of motion. The linearized equations for the kth blade will have periodic coefficients, since the kth blade equations are written in the blade-fixed rotating coordinate system.

3) The linearized equations with periodic coefficients are transformed into equations with constant coefficients by applying the multiblade coordinate transformation.[6]

4) The eigenvalues of the linearized system with constant coefficients are evaluated. The eigenvalues appear as complex conjugate pairs $s = \sigma \pm i\omega$. The mode is stable if σ is negative and unstable when σ is positive.

For the present problem there are six pairs of complex eigenvalues; each one representing one of the six degrees of freedom, namely, β_{1c}, β_{1s}, ζ_{1c}, ζ_{1s}, θ, and ϕ. The modes corresponding to the rotor degrees of freedom (β_{1c}, β_{1s}, ζ_{1c}, ζ_{1s}) are referred to as either a progressing or regressing mode. The designation of progressing or regressing for a particular mode is based on the numerical value of the rotating natural frequency of the rotor. Suppose the rotating natural frequency, say, in lead-lag, is f/rev. Then the two frequencies corresponding to the cyclic lag modes (ζ_{1c}, ζ_{1s}) will be $(f+1)$/rev and $(f-1)$/rev, where $f+1$ is the high-frequency lag mode and $f-1$ is the low-frequency lag mode. If f is greater than 1/rev, the high-frequency lag mode $(f+1)$ is a progressing mode and the low-frequency lag mode $(f-1)$ is a regressing mode. On the other hand, if f is less than 1/rev, the high-frequency lag mode is a progressing mode and the low-frequency lag mode is also a progressing mode. These designations are also applicable to the flap modes of the rotor. A clear description of these is given in Ref. 6. For a stiff in-plane rotor, the rotating natural frequency in lead-lag is greater than 1/rev. Hence the high-frequency lead-lag mode is a progressing mode and the low-frequency lead-lag mode is a regressing mode. For a soft in-plane rotor, since the rotating natural frequency is less than 1/rev, both high- and low-frequency lag modes are progressing modes.

The blade equations of equilibrium, the linearized perturbational blade equations, and the perturbational equations of motion in the pitch and roll degrees of freedom are presented in Appendix A. Certain differences, discussed below, exist between the equations used in Refs. 4 and 5 and those employed in this study. The equations used in this study[2] are based upon a flap-lag sequence of rotations, which relate the undeformed and deformed blade coordinate systems. The analytical model used in Ref. 4 was based on the theory presented in Ref. 10, where a lag-flap sequence was used. It can be shown that different hinge sequences lead to different transformation matrices; however, it was shown in Ref. 11 that blade stability does not depend on the hinge sequence when the equations are carefully derived. The equations used by Johnson[5] are documented in Ref. 7. The theory derived in Ref. 7 is not a moderate deflection theory and the transformation matrix, which is based on small-deflection theory, is the same for both flap-lag and lag-flap hinge sequences. It should be noted that coupled rotor/body equations usually consist of a considerable number of terms. Therefore, it seems reasonable to use agreement between theoretical predictions, based on these equations, and experimental data as an indication of the accuracy of the mathematical model.

Results and Discussion

In the present study, the aeromechanical stability of the helicopter model described previously is studied at various values of the rotor speed of rotation Ω. Thus, due to the

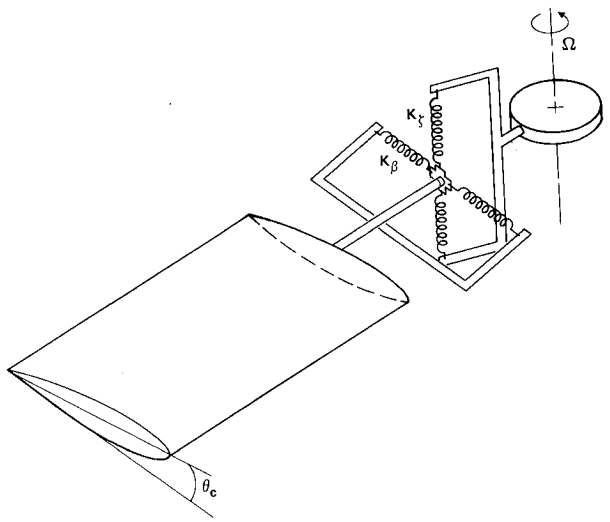

Fig. 1 Equivalent spring restrained blade model.

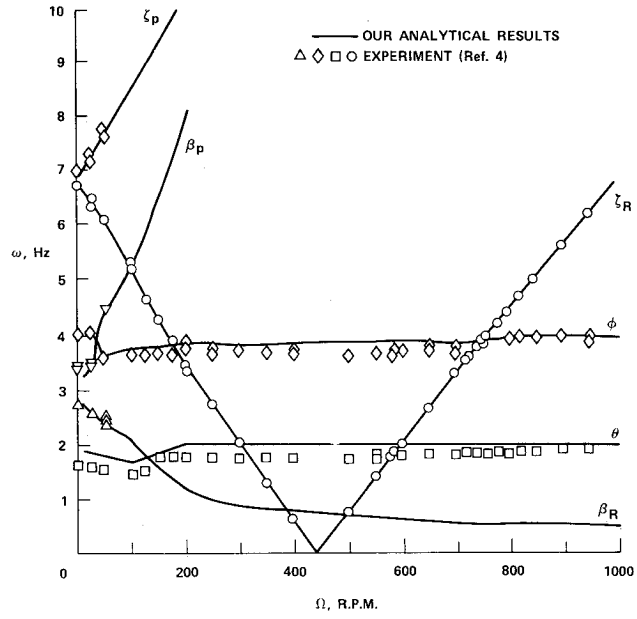

Fig. 2 Modal frequencies as a function of Ω; $\theta_c = 0$ (Configuration 1).

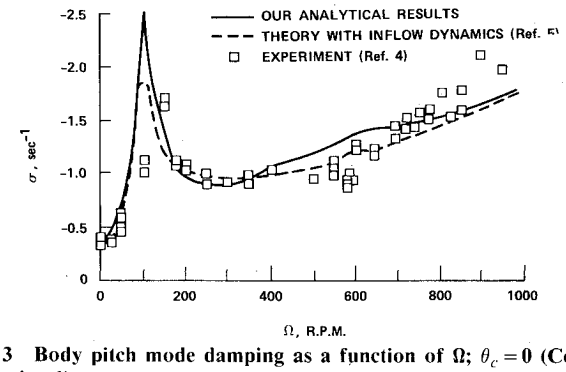

Fig. 3 Body pitch mode damping as a function of Ω; $\theta_c = 0$ (Configuration 1).

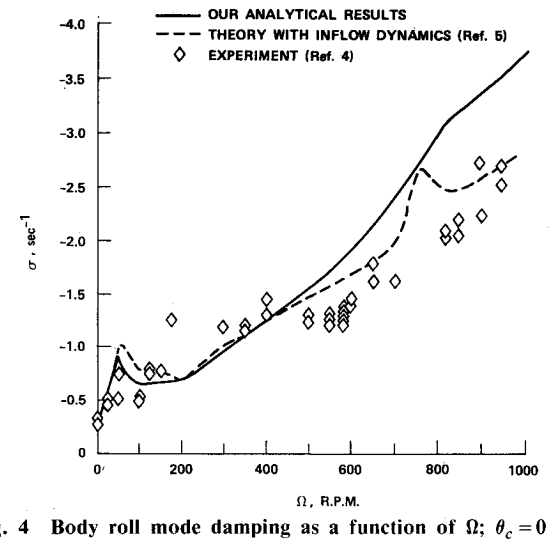

Fig. 4 Body roll mode damping as a function of Ω; $\theta_c = 0$ (Configuration 1).

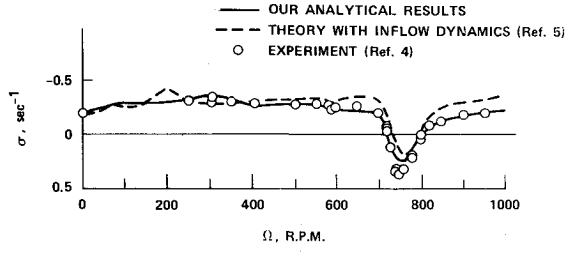

Fig. 5 Regressing lag mode damping as a function of Ω; $\theta_c = 0$ (Configuration 1).

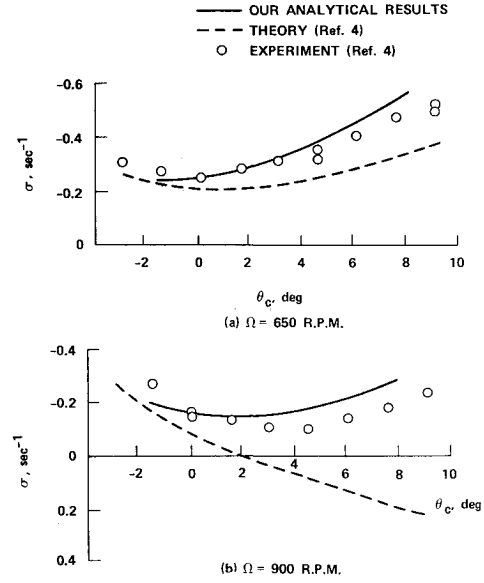

Fig. 6 Lead-lag regressing mode damping as a function of θ_c at a) 650 rpm and b) 900 rpm (Configuration 1).

variation in Ω, a stiff in-plane rotor at low Ω will become a soft in-plane rotor at high Ω. In the experiment performed by Bousman,[4] the flexibility of the blade in lead-lag is such that the rotor becomes a soft in-plane rotor beyond Ω = 445 rpm. Hence, for Ω < 445 rpm, the lead-lag modes will have one progressing mode and one regressing mode and for Ω > 445 rpm, both the lag modes will be progressing modes. In Refs. 4 and 5, even for Ω > 445 rpm, the low-frequency lag mode is referred to as regressing mode instead of progressing mode. So, for the sake of consistency, during the discussion of our results, the low-frequency lag mode is always referred to as lag regressing mode.

The results for Configuration 1 are presented in Figs. 2-7, while the results for Configuration 4 are presented in Figs. 8-12. The variation of the various model frequencies with Ω are presented in Fig. 2, together with the experimental data obtained in Ref. 4. The progressing flap and progressing lead-lag frequencies increase very rapidly with Ω. The lead-lag regressing mode frequency evaluated from the analytical model is in excellent agreement with the experimental results. The body pitch and roll frequencies have slightly higher values than the experimental results. The damping in pitch as a function Ω is shown in Fig. 3. The analytical results are in relatively good agreement with the experimental data. The variation of the damping in roll as a function of Ω is shown in Fig. 4. It is evident that for this case the analytical results yield values which are somewhat higher than the experimental data.

Figure 5 represents the variation of damping in lead-lag regressing mode with Ω. As indicated previously, Johnson's results[5] show that the theory with inflow dynamics shows better agreement with experimental data than the theory with quasisteady aerodynamics. However, even with quasisteady aerodynamics, the results of the present analysis show slightly better agreement than the results obtained in Ref. 5 with inflow dynamics. It is also important to note that in the region beyond 800 rpm, our results are in excellent agreement with the experimental data, while the theory with inflow dynamics predicts higher values.

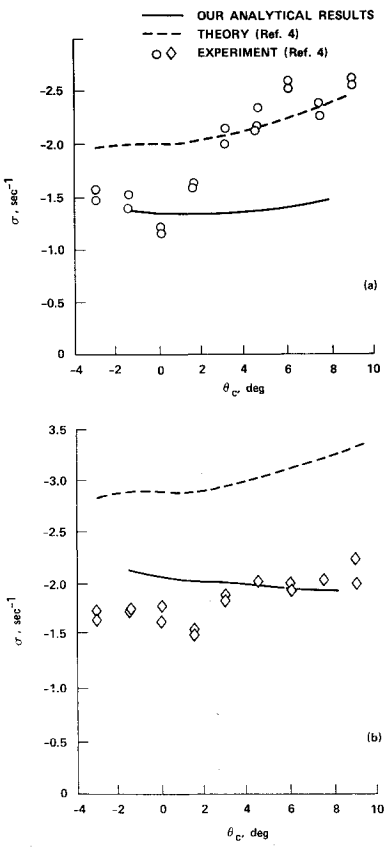

Fig. 7 Variation of damping in a) pitch and b) roll with θ_c at $\Omega = 650$ rpm (Configuration 1).

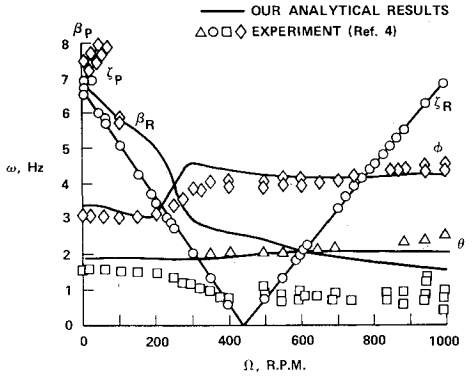

Fig. 8 Variation of modal frequencies with Ω; $\theta_c = 0$ (Configuration 4).

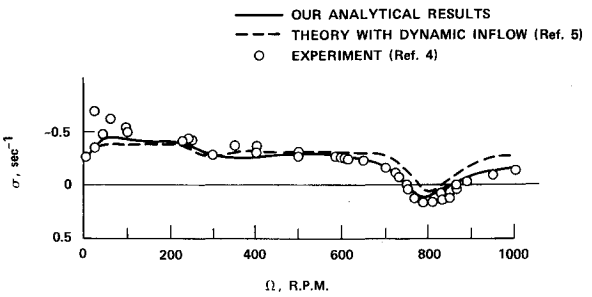

Fig. 9 Variation of damping in lag regressing mode with Ω; $\theta_c = 0$ (Configuration 4).

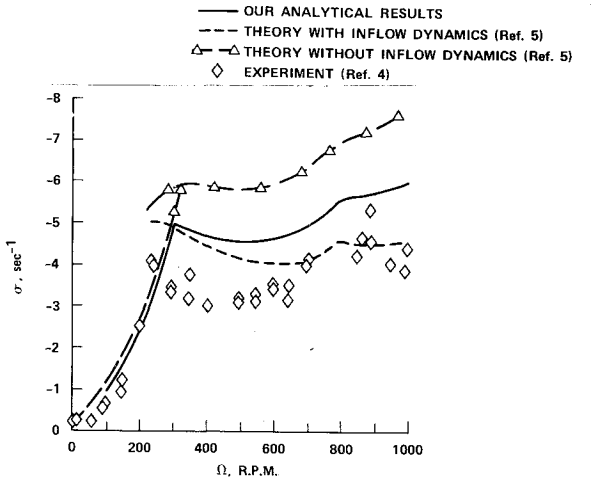

Fig. 10 Variation of damping in roll with Ω; $\theta_c = 0$ (Configuration 4).

Results from the calculations performed indicated that the progressing and regressing flap modes are always stable and the damping in these modes increases monotonically with Ω for Configuration 1 as well as for Configuration 4. Since these modes are always stable, the results are not presented herein.

Changes in the damping of the lead-lag regressing mode as a function of the collective pitch setting of the blade are presented in Fig. 6. Since Johnson[5] has not presented a corresponding set of results, it was not possible to compare these results with an analysis based on the dynamic inflow model. At $\Omega = 650$ rpm, the results shown in Fig. 6a indicate that the theoretical analysis used by Bousman[4] predicts a much lower value for the damping than the experimental results. The present analysis shows considerably better agreement. It should be noted, however, that for larger values of pitch setting the difference between the predicted results and the experimental results increases. This difference could be attributed to the simple quasisteady aerodynamic model used in our analysis. However, this difference is much smaller than the one exhibited by Bousman's results. Even more interesting are the results presented in Fig. 6b, corresponding to $\Omega = 900$ rpm. For this case experimental results indicate a lead-lag regressing mode which is always stable, but the theoretical results shown by Bousman[4] imply an instability which becomes stronger beyond a collective pitch setting of 2 deg. As evident from Fig. 6b, the results of our analysis predict the correct trend, and the predicted damping levels are much closer to the experimental results. It should be noted again that the agreement between the predicted and experimental results diminishes with increasing collective pitch setting.

The variations in pitch damping as a function of collective pitch setting are shown in Fig. 7a, and similar variations for roll damping are shown in Fig. 7b. As evident from Fig. 7b, the damping in roll is predicted quite well. However, the damping in pitch predicted by the present analysis is much lower than the experimental results. One can only speculate on the possible cause for this discrepancy. One possible reason could be the slight nonlinearity present in the structural damping in pitch mentioned in Ref. 4. At $\Omega = 650$ rpm, the lead-lag regressing mode frequency is close to the body pitch frequency (Fig. 2) and, therefore, the amplitudes in pitch could be higher. Thus, nonlinearity in structural damping in pitch could manifest itself by increasing the total damping in pitch.

The results for Configuration 4 are presented next. The variation of model frequencies with Ω are shown in Fig. 8. The lead-lag regressing mode frequency is in excellent agreement with our analytical predictions. The pitch and roll frequencies are predicted well. Bousman's[4] experiments showed the

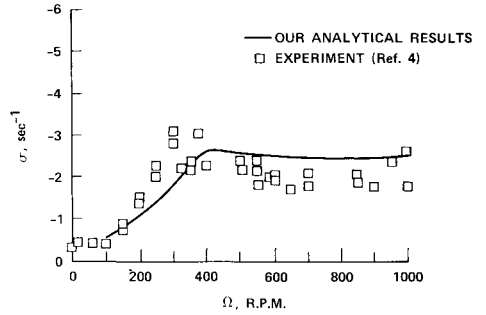

Fig. 11 Variation of damping in pitch with Ω; $\theta_c = 0$ (Configuration 4).

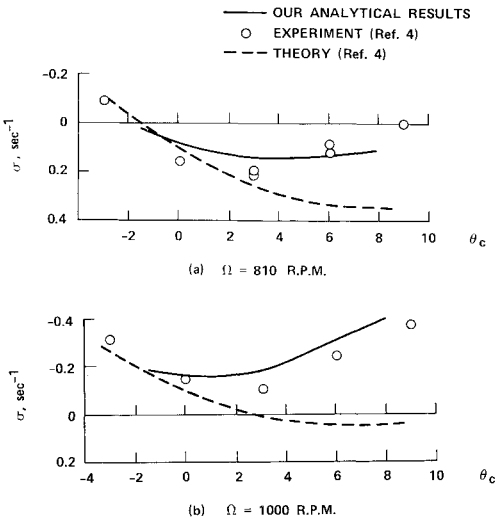

Fig. 12 Variation of damping in lag regressing mode with θ_c at a) 810 rpm and b) 1000 rpm (Configuration 4).

presence of a frequency of about 0.8 Hz beyond Ω = 350 rpm, whereas the present analysis has not predicted any frequency close to this value. However, Johnson,[5] using the *inflow dynamics model*, predicted theoretically a frequency close to 0.8 Hz and called it the inflow mode.

The variation of lead-lag regressing mode damping with Ω is presented in Fig. 9. Again, the present analytical results are in closer agreement with the experimental results than those predicted by the theory with inflow dynamics. Figures 10 and 11 show the variation of damping in roll and pitch modes with Ω. The pitch damping is predicted well. The roll damping is overestimated.

The variation in damping levels of the lead-lag regressing mode with collective pitch angle of the blade are shown in Fig. 12 for two different values of angular speed. It is evident from Fig. 12b that, for the case of Ω = 1000 rpm, the theory used by Bousman predicts an unstable region beyond $\theta_c = 3$ deg, however, the experiment indicates a stable configuration. The results of the present analysis are in good agreement with the experimental results. The agreement noted in Figs. 6 and 12, between the analytical results of our study and the experimental data, for nonzero values of collective pitch, seems to indicate that the discrepancy between theory and experiment for these cases, evident in Ref. 4, could be associated with the details of the mathematical model and is not related to unsteady aerodynamic effects such as dynamic inflow.

Concluding Remarks

In this paper, the results of a theoretical l nalysis of the aeromechanical stability of a hingeless rotor helicopter are compared with the experimental results. Using a quasisteady aerodynamic model, it was found that the results of the present analysis compare quite well with the experimental results. It is interesting to note that this correlation with experimental data appears to hold in both the region of zero collective pitch angles considered by Johnson,[5] as well as in the nonzero range of collective pitch angles considered by Bousman,[4] but not by Johnson. Obviously the quasisteady aerodynamic model is incapable of predicting the "dynamic inflow mode" which is caused by the augmented state of the system when the dynamic inflow model is used. In an extension of this study which will include dynamic inflow, the physical meaning of the dynamic inflow mode will be re-examined.

This study also indicates that the discrepancy between the predicted values of regressing mode lag damping and the experimental measurements, noted in Ref. 4 for Configurations 1 and 4, do not seem to be associated with dynamic inflow and are more likely to be related to the details of the mathematical model. Further, the analytical model used in this study has the capability of simulating the experiment, with good accuracy, because it is based on the same blade model which was actually tested.

Finally, it should be noted that the analytical model was based on an ordering scheme where blade slopes were assumed to be of order ϵ and the fuselage rotations in pitch and roll were assumed to be of order $\epsilon^{3/2}$, which leads to simplification in the equations of motion. The cases considered in the present study (both experimental and theoretical) were restricted so that only the linear first-order terms in fuselage rotations were important. Thus, other classes of problems, in which nonlinear terms in fuselage rotations are also exercised, have to be considered to determine the overall reliability of this particular ordering scheme.

Appendix: Equations Used in this Study

The equations of blade equilibrium, the linearized perturbational blade equations in multiblade coordinates, together with the perturbational equations in the pitch and roll degrees of freedom, are given below.

Equilibrium Equations

Flap:

$$\beta_0\left\{\bar{\omega}_F^2 + (\bar{\omega}_L^2 - \bar{\omega}_F^2)\sin^2\theta_c + \frac{\bar{\ell}^3}{3} + \frac{\bar{\ell}^2}{2}\bar{e}\right\} + \zeta_0\left\{(\bar{\omega}_L^2 - \bar{\omega}_F^2)\sin\theta_c\cos\theta_c + \nu\frac{\bar{\ell}^4}{4}\beta_p\right\} + \beta_0\zeta_0\left\{\nu\frac{\bar{\ell}^4}{4}\right\} + \beta_p\left\{\frac{\bar{\ell}^3}{3} + \frac{\bar{\ell}^2}{2}\bar{e}\right\} - \nu\left\{\frac{\bar{\ell}^4}{4}\theta_0 + \frac{\bar{\ell}^3}{3}(-\lambda + 2\bar{e}\theta_0) - \frac{\bar{\ell}^2}{2}\bar{e}\lambda\right\} = 0 \quad \text{(A1)}$$

Lead-Lag

$$\beta_0\{-(\bar{\omega}_L^2 - \bar{\omega}_F^2)\sin\theta_c\cos\theta_c\} + \zeta_0\left\{-\bar{\omega}^2{}_L + (\bar{\omega}^2{}_L - \bar{\omega}^2{}_F)\sin^2\theta_c - \frac{\bar{\ell}^2}{2}\bar{e} + \nu\left(-\frac{\bar{\ell}^4}{4}\beta_p\theta_0 - \frac{\bar{\ell}^3}{3}2\lambda\beta_p\right)\right\} + \beta_0\zeta_0\left\{\nu\frac{\bar{\ell}^3}{3}\lambda\right\} + \nu\left\{-\frac{c_{d0}}{a}\left(\frac{\bar{\ell}^4}{4} + 2\frac{\bar{\ell}^3}{3}\bar{e}\right) - \frac{\bar{\ell}^3}{3}\lambda\theta_0 + \frac{\bar{\ell}^2}{2}\lambda(\lambda - \bar{e}\theta_0)\right\} = 0 \quad \text{(A2)}$$

When there is no structural flap-lag coupling, the terms containing $\sin\theta_c$ and $\cos\theta_c$ must be deleted from the above equations as well as the stability equations given below.

Linearized Stability Equations

n cosine Flap

$$\beta_{nc}F_{nc}(1) + \beta_{ns}F_{nc}(2) + \zeta_{nc}F_{nc}(3) + \zeta_{ns}F_{nc}(4) + \dot{\beta}_{nc}F_{nc}(5) + \dot{\beta}_{ns}F_{nc}(6) + \dot{\zeta}_{nc}F_{nc}(7) + \ddot{\beta}_{nc}F_{nc}(8) + \ddot{\theta}F_{nc}(9) + \dot{\theta}F_{nc}(10) + \dot{\phi}F_{nc}(11) = 0 \quad \text{(A3)}$$

where

$$F_{nc}(1) = \bar{\omega}_F^2 + (\bar{\omega}_L^2 - \bar{\omega}_F^2)\sin^2\theta_c + \nu\frac{\bar{\ell}^4}{4}\zeta_0 + \frac{\bar{\ell}^3}{3} + \frac{\bar{\ell}^2}{2}\bar{e} - n^2\frac{\bar{\ell}^3}{3} - n^2\frac{1}{2}\nu\bar{b}\frac{\bar{\ell}^3}{3}\cos\theta_0$$

$$F_{nc}(2) = n\left(\nu\frac{\bar{\ell}^4}{4} + \nu\frac{\bar{\ell}^3}{3}\bar{e} + \bar{g}_{SF}\right)$$

$$F_{nc}(3) = (\bar{\omega}_L^2 - \bar{\omega}_F^2)\sin\theta_c + \cos\theta_c + \nu\frac{\bar{\ell}^4}{4}(\beta_p + \beta_0)$$

$$F_{nc}(4) = \left[2\frac{\bar{\ell}^3}{3}(\beta_0 + \beta_p) - 2\nu\frac{\bar{\ell}^4}{4}\theta_0 + \nu\frac{\bar{\ell}^3}{3}\lambda\right]n$$

$$F_{nc}(5) = \nu\frac{\bar{\ell}^4}{4} + \nu\frac{\bar{\ell}^3}{3}\bar{e} + \bar{g}_{SF}$$

$$F_{nc}(6) = n\left[2\frac{\bar{\ell}^3}{3} + \nu\frac{\bar{\ell}^3}{3}\bar{b}\cos\theta_0\right]$$

$$F_{nc}(7) = 2\frac{\bar{\ell}^3}{3}(\beta_0 + \beta_p) - 2\nu\frac{\bar{\ell}^4}{4}\theta_0 + \nu\frac{\bar{\ell}^3}{3}\lambda$$

$$F_{nc}(8) = \frac{\bar{\ell}^3}{3} + \frac{1}{2}\nu\bar{b}\frac{\bar{\ell}^3}{3}\cos\theta_0$$

$$F_{nc}(9) = -\frac{\bar{\ell}^3}{3}\delta_n$$

$$F_{nc}(10) = -\delta_n\nu\frac{\bar{\ell}^4}{4}$$

$$F_{nc}(11) = \delta_n\left[2\frac{\bar{\ell}^3}{3} + \bar{h}_2\left(2\nu\frac{\bar{\ell}^3}{3}\theta_0 - \nu\frac{\bar{\ell}^2}{2}\lambda\right)\right]$$

where

$\delta_n = 1$ when $n = 1$

$= 0$ when $n \neq 1$

n sine Flap

$$\beta_{ns}F_{nc}(1) - \beta_{nc}F_{nc}(2) + \zeta_{ns}F_{nc}(3) - \zeta_{nc}F_{nc}(4) + \dot{\beta}_{ns}F_{nc}(5) - \dot{\beta}_{nc}F_{nc}(6) + \dot{\zeta}_{ns}F_{nc}(7) + \ddot{\beta}_{ns}F_{nc}(8) - \ddot{\phi}F_{nc}(9) - \dot{\phi}F_{nc}(10) + \dot{\theta}F_{nc}(11) = 0 \quad \text{(A4)}$$

n cosine Lead-Lag

$$\zeta_{nc}L_{nc}(1) + \zeta_{ns}L_{nc}(2) + \beta_{nc}L_{nc}(3) + \beta_{ns}L_{nc}(4) + \dot{\zeta}_{nc}L_{nc}(5) + \dot{\zeta}_{ns}L_{nc}(6) + \dot{\beta}_{nc}L_{nc}(7) + \dot{\beta}_{ns}L_{nc}(8) + \ddot{\zeta}_{nc}L_{nc}(9) + \ddot{\beta}_{nc}L_{nc}(10) + \ddot{\phi}L_{nc}(11) + \ddot{\theta}L_{nc}(12) + \dot{\theta}L_{nc}(13) = 0 \quad \text{(A5)}$$

where

$$L_{nc}(1) = -\bar{\omega}_L^2 + (\bar{\omega}_L^2 - \bar{\omega}_F^2)\sin^2\theta_c - \frac{\bar{\ell}^2}{2}\bar{e} + n^2\frac{\bar{\ell}^3}{3} - \nu\frac{\bar{\ell}^4}{4}\beta_p\theta_0$$

$$L_{nc}(2) = -n\left[2\nu\frac{c_{d0}}{a}\frac{\bar{\ell}^4}{4} + \nu\frac{\bar{\ell}^3}{3}\theta_0\lambda + \bar{g}_{SL}\right]$$

$$L_{nc}(3) = -(\bar{\omega}_L^2 - \bar{\omega}_F^2)\sin\theta_c\cos\theta_c - n^2\frac{1}{2}\nu\bar{b}\frac{\bar{\ell}^3}{3}\sin\theta_0$$

$$L_{nc}(4) = n\left[2\frac{\bar{\ell}^3}{3}(\beta_0 + \beta_p) - \nu\frac{\bar{\ell}^4}{4}\theta_0 - \nu\frac{\bar{\ell}^3}{3}(-2\lambda + \bar{e}\theta_0)\right]$$

$$L_{nc}(5) = -2\nu\frac{c_{d0}}{a}\frac{\bar{\ell}^4}{4} - \nu\frac{\bar{\ell}^3}{3}\theta_0\lambda - \bar{g}_{SL}$$

$$L_{nc}(6) = -n\,2\frac{\bar{\ell}^3}{3}$$

$$L_{nc}(7) = 2\frac{\bar{\ell}^3}{3}(\beta_0 + \beta_p) - \nu\frac{\bar{\ell}^4}{4}\theta_0 - \nu\frac{\bar{\ell}^3}{3}(-2\lambda + \bar{e}\theta_0)$$

$$L_{nc}(8) = 2n\frac{1}{2}\nu\bar{b}\frac{\bar{\ell}^3}{3}\sin\theta_0$$

$$L_{nc}(9) = -\frac{\bar{\ell}^3}{3}$$

$$L_{nc}(10) = \frac{1}{2}\nu\bar{b}\frac{\bar{\ell}^3}{3}\sin\theta_0$$

$$L_{nc}(11) = \delta_n\left\{\frac{\bar{\ell}^3}{3}(\beta_p + \beta_0) + \bar{h}_2\frac{\bar{\ell}^2}{2}\right\}$$

$$L_{nc}(12) = \delta_n\bar{h}_2\frac{\bar{\ell}^2}{2}\zeta_0$$

$$L_{nc}(13) = \delta_n\left\{\nu\frac{\bar{\ell}^4}{4}\theta_0 - \frac{\bar{\ell}^3}{3}2\lambda\nu\right\}$$

n sine Lead-Lag

$$\zeta_{ns}L_{nc}(1) - \zeta_{nc}L_{nc}(2) + \beta_{ns}L_{nc}(3) - \beta_{nc}L_{nc}(4) + \dot{\zeta}_{ns}L_{nc}(5) - \dot{\zeta}_{nc}L_{nc}(6) + \dot{\beta}_{ns}L_{nc}(7) - \dot{\beta}_{nc}L_{nc}(8) + \ddot{\zeta}_{ns}L_{nc}(9) + \ddot{\beta}_{ns}L_{nc}(10) + \ddot{\theta}L_{nc}(11) - \ddot{\phi}L_{nc}(12) - \dot{\phi}L_{nc}(13) = 0 \quad \text{(A6)}$$

Roll

$$\frac{N}{2}m\Omega^2R^3[\beta_{1c}R(1) + \beta_{1s}R(2) + \zeta_{1c}R(3) + \zeta_{1s}R(4) + \dot{\beta}_{1c}R(5) + \dot{\beta}_{1s}R(6) + \dot{\zeta}_{1c}R(7) + \dot{\zeta}_{1s}R(8) + \ddot{\beta}_{1c}R(9) + \ddot{\beta}_{1s}R(10) + \ddot{\zeta}_{1c}R(11) + \ddot{\phi}R(12) + \dot{\phi}R(13) + \ddot{\theta}R(14) + \dot{\theta}R(15)] - I_{xx}\Omega^2\ddot{\phi} + I_{xy}\Omega^2\ddot{\theta} = 0 \quad \text{(A7)}$$

$$R(1) = \nu\frac{c_{d0}}{a}\frac{\bar{\ell}^4}{4} + \nu\frac{\bar{\ell}^3}{3}\lambda\theta_0 + \bar{g}_{SF} + \nu\frac{\bar{\ell}^4}{4} + 2\nu\frac{\bar{\ell}^3}{3}\bar{e} + \bar{h}_2\left[\nu\frac{\bar{\ell}^3}{3}(\beta_p + \beta_0) + \nu\frac{\bar{\ell}^3}{3}\theta_0\zeta_0 + \frac{1}{2}\nu\bar{b}\frac{\bar{\ell}^2}{2}\sin\theta_0\right]$$

$$R(2) = -2\nu\frac{\bar{\ell}^4}{4}\zeta_0 + \nu\frac{\bar{\ell}^4}{4}(\beta_p + \beta_0)\theta_0 + \frac{1}{2}\nu\bar{b}\frac{\bar{\ell}^3}{3}\cos\theta_0 + \bar{h}_2\left[2\nu\frac{\bar{\ell}^3}{3}\theta_0 - \bar{\ell}^2\beta_0 - \bar{\ell}^2\beta_p + \nu\frac{\bar{\ell}^2}{2}(-3\lambda + \bar{e}\theta_0)\right]$$

$$R(3) = -\nu\frac{\bar{\ell}^4}{4}\theta_0 - \bar{h}_2\nu\frac{\bar{\ell}^3}{3}\theta_0(\beta_p + \beta_0)$$

$$R(4) = \nu\frac{\bar{\ell}^4}{4}\zeta_0 2\theta_0 - \nu\frac{\bar{\ell}^4}{4}(\beta_p + \beta_0) + \beta_p\bar{g}_{SL} - \bar{h}_2\left(\bar{\ell}^2\zeta_0 - 2\nu\frac{c_{d0}}{a}\frac{\bar{\ell}^3}{3} - \nu\frac{\bar{\ell}^3}{3}\lambda\theta_0\right)$$

$$R(5) = -\nu\frac{\bar{\ell}^4}{4}\zeta_0 + \nu\frac{\bar{\ell}^4}{4}(\beta_0+\beta_p)\theta_0 + 2\frac{\bar{\ell}^3}{3} + 2\frac{\bar{\ell}^2}{2}\bar{e} + \nu\bar{b}\frac{\bar{\ell}^3}{3}\cos\theta_0$$
$$-\bar{h}_2\left[\bar{\ell}^2(\beta_0+\beta_p) - \nu\frac{\bar{\ell}^3}{3}\theta_0 - \nu\frac{\bar{\ell}^2}{2}(-2\lambda+\bar{e}\theta_0)\right]$$

$$R(6) = -2\frac{\bar{\ell}^3}{3}\zeta_0 - \bar{g}_{SF} - \nu\frac{\bar{\ell}^4}{4} - 2\nu\frac{\bar{\ell}^3}{3}\bar{e}$$
$$-\bar{h}_2\left[\nu\frac{\bar{\ell}^3}{3}(\beta_0+\beta_p) + \nu\bar{b}\frac{\bar{\ell}^2}{2}\sin\theta_0\right]$$

$$R(7) = \nu\frac{\bar{\ell}^4}{4}\zeta_0 2\theta_0 + \beta_p\bar{g}_{SL} - \bar{h}_2$$
$$\times\left[\bar{\ell}^2\zeta_0 - 2\nu\frac{c_{d0}}{a}\frac{\bar{\ell}^3}{3} - \nu\frac{\bar{\ell}^2}{2}\lambda\theta_0\right]$$

$$R(8) = 2\nu\frac{\bar{\ell}^4}{4}\theta_0 - \nu\frac{\bar{\ell}^3}{3}\lambda + 2\nu\frac{\bar{\ell}^3}{3}\bar{e}\theta_0 + \bar{h}_2\left[\nu\frac{\bar{\ell}^3}{3}2\theta_0(\beta_p+\beta_0)\right]$$

$$R(9) = -\frac{\bar{\ell}^3}{3}\zeta_0 - \bar{h}_2\frac{1}{2}\nu\bar{b}\frac{\bar{\ell}^2}{2}\sin\theta_0$$

$$R(10) = -\frac{\bar{\ell}^3}{3} - \frac{1}{2}\nu\bar{b}\frac{\bar{\ell}^3}{3}\cos\theta_0 - \frac{\bar{\ell}^2}{2}\bar{e} - \bar{h}_2\frac{\bar{\ell}^2}{2}(\beta_p+\beta_0)$$

$$R(11) = \frac{\bar{\ell}^3}{3}(\beta_p+\beta_0) + \bar{h}_2\frac{\bar{\ell}^2}{2}$$

$$R(12) = -\frac{\bar{\ell}^3}{3} - \frac{\bar{\ell}^2}{2}\bar{e} - \bar{h}_2\frac{\bar{\ell}^2}{2}(\beta_p+\beta_0)$$
$$-\bar{h}_2\left[\frac{\bar{\ell}^2}{2}(\beta_p+\beta_0) + 2\bar{h}_2\bar{\ell}\right]$$

$$R(13) = -\frac{\bar{\ell}^3}{3}2\zeta_0 - \nu\frac{\bar{\ell}^3}{3}\bar{e} - \nu\frac{\bar{\ell}^4}{4} - \bar{h}_2\nu\frac{\bar{\ell}^3}{3}(\beta_p+\beta_0)$$

$$R(14) = \frac{\bar{\ell}^3}{3}\zeta_0$$

$$R(15) = \nu\frac{\bar{\ell}^4}{4}\zeta_0 - 2\frac{\bar{\ell}^3}{3} - \frac{\bar{\ell}^2}{2}2\bar{e} - \bar{h}_2\nu\frac{\bar{\ell}^3}{3}\theta_0 + \nu\frac{\bar{\ell}^2}{2}3\lambda\bar{h}_2 - \bar{h}_2\nu\frac{\bar{\ell}^3}{3}2\theta_0$$

Pitch

$$(N/2)m\Omega^2R^3[-R(2)\beta_{1c} + R(1)\beta_{1s} - R(4)\zeta_{1c} + R(3)\zeta_{1s}$$
$$-R(6)\dot{\beta}_{1c} + R(5)\dot{\beta}_{1s} - R(8)\dot{\zeta}_{1c} + R(7)\dot{\zeta}_{1s} - R(10)\ddot{\beta}_{1c}$$
$$+R(9)\ddot{\beta}_{1s} + R(11)\ddot{\zeta}_{1s} - R(14)\ddot{\phi} - R(15)\dot{\phi} + R(12)\ddot{\theta}$$
$$+R(13)\dot{\theta}] - I_{yy}\ddot{\theta}\Omega^2 + I_{yx}\ddot{\phi}\Omega^2 = 0 \qquad \text{(A8)}$$

Acknowledgments

This study was supported by NASA Ames Research Center under Grant NAG 2-116. The authors would like to express their gratitude to W. G. Bousman, W. Johnson, and H. Miura for the constructive comments they have made on the draft version of this paper.

References

[1] Friedmann, P. P., "Formulation and Solution of Rotary-Wing Aeroelastic Stability and Response Problems," *Vertica*, Vol. 7, No. 2, 1983, pp. 101-141.

[2] Venkatesan, C. and Friedmann, P. P., "Aeroelastic Effects in Multirotor Vehicles with Application to Hybrid Heavy Lift System, Part I: Formulation of Equations of Motion," NASA CR 3822, Aug. 1984.

[3] Venkatesan, C. and Friedmann, P. P., "Aeroelastic Effects in Multirotor Vehicles, Part II: Method of Solution and Results Illustrating Coupled Rotor/Body Aeromechanical Stability," NASA CR under review.

[4] Bousman, W. G., "An Experimental Investigation of the Effects of Aeroelastic Couplings on Aeromechanical Stability of a Hingeless Rotor Helicopter," *Journal of the American Helicopter Society*, Vol. 26, Jan. 1981, pp. 46-54.

[5] Johnson, W., "Influence of Unsteady Aerodynamics on Hingeless Rotor Ground Resonance," *Journal of Aircraft*, Vol. 19, Aug. 1982, pp. 668-673.

[6] Johnson, W., *Helicopter Theory*, Princeton University Press, Princeton, N. J., 1980.

[7] Johnson, W., "A Comprehensive Analytical Model of Rotorcraft Aerodynamics and Dynamics," NASA TM 81182, June 1980.

[8] Friedmann, P. and Venkatesan, C., "Comparison of Experimental Coupled Helicopter Rotor/Body Stability Results with a Simple Analytical Model," presented at the Integrated Technology Rotor (ITR) Methodology Assessment Workshop, NASA Ames Research Center, Moffett Field, Calif., June 1983.

[9] Greenberg, J. M., "Airfoil in Sinusoidal Motion in a Pulsating Flow," NACA TN 1326, 1947.

[10] Hodges, D. H., "A Theoretical Technique for Analyzing Aeroelastic Stability of Bearingless Rotors," *Proceedings of the 19th AIAA/ASME Structures, Structural Dynamics and Materials Conference*, April 1978, pp. 282-294.

[11] Hodges, D. H., Ormiston, R. A., and Peters, D. A., "On the Non-Linear Deformation Geometry of Euler-Bernoulli Beams," NASA TP 1566, 1980.